Polymer Chemistry

Accepted Manuscript

ROYAL SOCIETY OF CHEMISTRY

www.rsc.org/polymers

Cite this: DOI: 10.1039/c0xx00000x

www.rsc.org/xxxxxx

ARTICLE TYPE

Design of coordination polymers with 4′-substituted functionalized terpyridyls in the backbone and pendent cyclopentadienyliron moieties

Alaa S. Abd-El-Aziz,*[a,b] Jessica L. Pilfold,[b] Badri Z. Momeni,[b,c] Adam J. Proud[a] and Jason K. Pearson[a]

Received (in XXX, XXX) XthXXXXXXXXX 20XX, Accepted Xth XXXXXXXXX 20XX

DOI: 10.1039/b000000x

The reaction of dichloro-terminated organoiron complex $[Fe(1,4\text{-}C_6H_4Cl_2)Cp]^+PF_6^-$ (**3**) with 4-hydroxybenzoic acid resulted in the formation of dicarboxylic acid organoiron complex **4**. 4′-Hexyl alcohol-2,2′:6′,2″-terpyridine (hextpy) **2** was reacted with dicarboxylic acid organoiron complex **4** or the similar monoacid organoiron complex **5** to afford two novel organoiron complexes containing one or two terminal terpyridine moieties (complexes **6** and **7**, respectively). Molecular dynamics simulations of **7** revealed that the terminal terpyridine units readily interact with one another. The metal-containing complexes $[M(hextpy)_2](PF_6)_2$ {M = Fe (**8**), Ni (**9**)} were prepared from the reaction of $FeCl_2{\cdot}4H_2O$ or $Ni(CH_3COO)_2{\cdot}4H_2O$ with hextpy **2**. The products were fully characterized by IR, UV-visible, NMR spectroscopy, and elemental analysis. The reaction of monocarboxylic acid organoiron complex **5** with bis(hextpy) complexes **8** and **9** afforded the novel chloro-terminated monomers **10** and **11** containing two different metals. The reaction of monomer **7** with iron(II) chloride or nickel(II) acetate in methanol produced iron(II)- or nickel(II)-containing polymers **12** (M = Fe) and **13** (M = Ni), respectively. The monomers containing multimetal centers were polymerized through aromatic substitution reactions with bisphenol A or hydroquinone to afford polymers **14** and **15**, respectively. The thermal properties of the polymers were also investigated, providing glass transition temperatures of approximately -25 ºC for the iron-chelated polymers and a stepwise degradation of the polymers, beginning with the decoordination of the pendent cationic iron moieties and ending with the loss of the bonding interaction between the iron center and the nitrogen atoms of the chelated terpyridine groups.

.

Introduction

The synthesis, characterization, and application of metal-containing polymers have been studied extensively in light of the wide variety of electrochemical, optical, magnetic, and catalytic properties that give these polymers such widespread potential applications in fields such as materials chemistry, biotechnology, and medicine. The degree of polymerization, type of bonding present, and the nature of the metal moiety have strong influences on these properties. Recent work in coordination polymer chemistry has shifted towards the development of materials that demonstrate particular physical properties, affording potential function in specific commercial applications.[1] The use of polydentate ligands in these coordination polymers has grown rapidly in the last decade, with 2,2′:6′,2″-terpyridine derivatives at the forefront, acting as tridentate pyridylligands.[2-13]

Easy synthetic access of 4′-substituted terpyridine derivatives affords the construction of a linear coordination motif with a strongly increased binding constant.[14-15] Schubert and coworkers demonstrated this property by preparing new terpyridine metal complexes with flexible oligomeric and polymeric spacers that revealed a strong relationship between the binding strength of the metal ion and the stability of the terpyridine metal complex.[10,12,16-19] Substituted terpyridine ligands are widely used as building blocks in supramolecular chemistry due to their abilities to readily coordinate to a variety of transition metal ions.[20-21] Two terpyridine ligands can chelate around a metal ion to form an octahedral complex, where the two outer rings rotate along the central C-C bonds connecting the rings to create a stable binding site through the lone pairs of the three nitrogen atoms. Upon coordination to an octahedral metal center, terpyridines functionalized at the 4′-position produce a rigid linear moiety, which can be used in the formation of molecular wires and rods.[22-27] Constable and Housecroft reported a variety of terpyridine ligands with diverse functional groups, or spacers, at the 4′-position, including ferrocene,[28] anthracene,[29] thienyl groups,[30,31] fluoro-substituted aryl groups,[32-33] and C_{60}-functionalized alkyl chains.[34] The corresponding coordination polymers can be tuned to have specific properties through variation of the metal ion used for complexation and the composition and length of the spacer unit, acting as an easily modified base for supramolecular architectures and metal-organic frameworks.[35] Terpyridine-based coordination polymers with photophysical and electrochemical properties have been prepared by altering the spacer between two terminal terpyridine units to include a fluorescent or electroactive functional group as well.[36]

In addition to chelation, terpyridine can undergo electrophilic aromatic substitution on any of its pyridyl rings, providing an efficient synthetic route for the preparation of substituted

terpyridine complexes. This work will focus on the synthesis of novel coordination polymers containing functionalized terpyridines substituted at the 4′-position. In addition to the metals chelated within the polymer backbones, the complexes also contain pendent cyclopentadienyliron moieties. We have previously described the incorporation of cyclopentadienyliron into polyethers, esters, norbornenes, and methacrylates with various functional groups.[37-41] The use of arene-coordinated cyclopentadienyliron moieties to enable nucleophilic aromatic substitution allows for an efficient method to chemically incorporate cationic metal groups into new materials.[42-48] The functionalization of the terpyridine moiety with established organoiron-containing complexes enables the formation of coordination polymers containing multiple metal centers, resulting in changes to their spectroscopic and thermal properties and therefore broadening the potential applications for these novel polymers.

Experimental

General Remarks

All reagents were purchased from Sigma-Aldrich, Alfa Aesar, or VWR, and used without further purification. All solvents were HPLC grade from Fisher Scientific and used without further purification. Elemental analyses were performed by a Perkin-Elmer 2400 II elemental analyzer. NMR spectral data were collected on a Varian Mercury Plus spectrometer 400 MHz. Chemical shifts were referenced to residual solvent peaks and coupling constants were reported in Hz. IR spectra were recorded on a Shimadzu IR Prestige-21 spectrophotometer with neat samples on a MIRacle A diamond ATR accessory from PIKE Technologies. UV-visible measurements were performed using a Shimadzu UV-2550 spectrophotometer at 25 ± 1 °C. Compounds **1**, **3**, and **5** were prepared by previously published procedures.[48-49]

Preparation of 4′-Hexyl Alcohol-2,2′:6′,2″-terpyridine, 2

The procedure was obtained by modifying and combining multiple established methods to optimize the reaction for both highest yield and purest product.[50-53] 1,6-Hexanediol (0.65 g, 5.5 mmol) was added to a stirred suspension of powdered KOH (0.31 g, 5.5 mmol) and dry DMSO (8 mL) under N_2 at 80 °C and the reaction was heated for 30 minutes. TpyCl **1** (0.27 g, 1 mmol) was added and the mixture was stirred for 4 h at 70 °C. The reaction was poured into water (75 mL) and extracted with dichloromethane. The organic product was dried with Na_2SO_4 and then the solvent was removed *in vacuo*. The product was isolated as a white powder. Yield: 86%.

Preparation of η^6-Dicarboxybenzene-η^5-cyclopentadienyliron Hexafluorophosphate, 4

Complex **3** (3.30 g, 8 mmol), 4-hydroxybenzoic acid (8.07 g, 64 mmol), and K_2CO_3 (16.58 g, 120 mmol) in 140 mL DMF were stirred under N_2 for 18 h in darkness. The reaction mixture was poured into 1.2 M HCl containing an equimetal molar amount of NH_4PF_6, which was extracted with dichloromethane and washed with water. The organic layer was dried with $MgSO_4$ and then the solvent was removed *in vacuo*. The resulting product was poured into diethyl ether and placed in the freezer overnight. The ether was decanted and the product was left to air-dry. The product was isolated as a yellow powder. Yield: 95%. Elemental analysis ($C_{25}H_{19}F_6FeO_6P$): calc. C 48.73%, H 3.11%; found, C 48.50%, H 3.02%. NMR data in acetone-d_6: $\delta(^1H)$ 8.17 (d, J = 8.7, 4H), 7.43 (d, J = 8.7, 4H), 6.59 (s, 4H), 5.43 (s, 5H). $\delta(^{13}C)$ 166.6, 158.5, 133.2, 130.8, 129.1, 120.7, 79.6, 77.7. IR: 1697 (C=O), 1288 (C-O acid), 1232, 1128 (aryl C-O-C). UV-vis:λ_{max}/nm (CH_3CN) 244.

Preparation of Complex 6

A mixture of hextpy **2** (0.35 g, 1 mmol), acid complex **5** (0.50 g, 1 mmol), N,N'-dicyclohexylcarbodiimide (0.52 g, 2.5 mmol), and N,N'-dimethylaminopyridine (0.32 g, 2.5 mmol) were stirred in dichloromethane (10 mL) under N_2 for 18 h in the dark. The solvent was removed *in vacuo* and the red precipitate was dissolved in a minimum amount of acetone. The solution was added dropwise to 1.2 M HCl containing an equimetal molar amount of NH_4PF_6 and cooled for 1 h. The precipitate was collected by filtration and washed with water. To remove unreacted acid complex **5**, the precipitate was washed with basic water. The product was isolated as a red solid. Yield: 90%. Elemental analysis ($C_{39}H_{35}ClF_6FeN_3O_4P$): calc. C 55.37%, H 4.17%, N 4.97%; found, C 55.18%, H 4.25%, N 4.90%. NMR data in DMSO-d_6: $\delta(^1H)$ 8.80 (m, 4H), 8.23 (t, J = 7.6, 2H), 8.11 (s, 2H), 8.10 (d, J = 8.7, 2H), 7.70 (t, J = 6.0, 2H), 7.41 (d, J = 8.7, 2H), 6.83 (d, J = 6.9, 2H), 6.53 (d, J = 6.9, 2H), 5.29 (s, 5H), 4.33 (m, 4H), 1.86 (m, 2H), 1.78 (m, 2H), 1.57-1.46 (m, 4H); $\delta(^{13}C)$ 167.5, 164.9, 157.1, 154.6, 152.2, 147.7, 140.0, 131.9, 130.7, 127.5, 125.6, 122.2, 120.4, 108.3, 104.0, 86.9, 79.6, 77.5, 68.5, 64.9, 28.3, 28.1, 25.2, 25.1. IR: 1710 (C=O), 1624, 1533, 1500, 1456 (C=C, C=N), 1357 (=C-N), 1278, 1161 (C-O-C ester). UV-vis: λ_{max}/nm (CH_3CN) 246, 277, 315, 325.

Preparation of Complex 7

The synthetic method for complex **7** is the same as that for complex **6**, with reagents in the following amounts: hextpy **2** (0.69 g, 2 mmol), diacid complex **4** (0.59 g, 1 mmol), N,N'-dicyclohexylcarbodiimide (0.82 g, 4 mmol), and N,N'-dimethylaminopyridine (0.50 g, 4 mmol) in dichloromethane (9 mL). The product was isolated as a pink precipitate. Yield: 80%. Elemental analysis ($C_{67}H_{61}F_6FeN_6O_8P$): calc. C 62.92%, H 4.81%, N 6.57 %; found, C 62.79%, H 4.76%, N 6.55%. NMR data in DMSO-d_6: $\delta(^1H)$ 8.80 (d, J = 4.7, 4H), 8.76 (d, J = 8.0, 4H), 8.19 (t, J = 7.7, 4H), 8.10 (d, J = 8.6, 4H), 8.08 (s, 4H), 7.67 (t, J = 6.1, 4H), 7.39 (d, J = 8.6, 4H), 6.43 (s, 4H), 5.26 (s, 5H), 4.32 (q, J = 13.2, 6.6, 8H), 1.85 (m, 4H), 1.78 (m, 4H), 1.46-1.57 (m, 8H); $\delta(^{13}C)$ 167.5, 164.9, 157.8, 154.1, 152.0, 147.6, 140.8, 131.8, 128.9, 127.2, 125.7, 122.3, 119.9, 108.3, 78.4, 76.6, 68.5, 64.8, 28.3, 28.1, 25.2, 25.0. IR: 1710 (C=O), 1624, 1535, 1473, 1435 (C=C, C=N), 1346 (=C-N), 1271, 1165 (C-O-C ester). UV-vis: λ_{max}/nm (CH_3CN) 245, 276, 315, 345.

Preparation of $[Fe(hextpy)_2][PF_6]_2$, 8

Hextpy **2** (0.69 g, 2 mmol) and $FeCl_2{\cdot}4H_2O$ (0.20 g, 1 mmol) were dissolved in methanol (25 mL) and stirred at room temperature for 30 min. The purple solution was poured into water containing a ten-fold molar excess of NH_4PF_6, and the resulting precipitate was filtered over Celite and washed with water, ethanol, and diethyl ether. The purple precipitate was dissolved in acetonitrile and the solvent was removed *in vacuo* to give a deep purple precipitate. Yield: 94%. Elemental analysis ($C_{42}H_{46}F_{12}FeN_6O_4P_2$): calc. C 48.29%, H 4.44%, N 8.05%; found, C 48.44%, H 4.36%, N 8.18%. NMR data in DMSO-d_6: $\delta(^1H)$ 8.93 (s, 4H), 8.83 (d, J = 8.0, 4H), 7.97 (td, J = 1.5, 7.8, 4H), 7.23 (d, J = 5.9, 4H), 7.17 (t, J = 7.1, 4H), 4.72 (m, 2H), 4.62 (t, J = 6.4, 4H), 3.49 (t, J = 6.0, 4H), 2.04 (q, J = 7.0, 4H), 1.66 (q, J = 6.9, 4H), 1.54 (m, 8H); $\delta(^{13}C)$ 167.6, 160.2, 157.9, 153.0, 138.5, 127.4, 123.7, 111.6, 70.0, 60.7, 32.6, 28.6, 25.5, 25.3. IR: 3597 (O-H), 1616, 1552, 1469, 1427 (C=C, C=N), 1365 (=C-N), 1217, 1041 (aryl C-O-CH_2). UV-vis: λ_{max}/nm (CH_3CN) 244, 271, 315, 365, 555.

Preparation of $[Ni(hextpy)_2][PF_6]_2$, 9

Hextpy **2** (0.69 g, 2 mmol) and $Ni(CH_3COO)_2.4H_2O$ (0.25 g, 1 mmol) were combined in methanol (42 mL) and stirred at room temperature for 1 h. The orange-pink solution was then poured into methanol (20 mL) containing a ten-fold molar excess of NH_4PF_6. The precipitate was filtered and washed with methanol and diethyl ether. The isolated product was a brown powder. Yield: 60 %. Elemental analysis ($C_{42}H_{46}F_{12}NiN_6O_4P_2$): calc. C 48.16 %, H 4.43 %, N 8.02 %; found, C 48.25 %, H 4.36 %, N 8.11 %.IR: 1600, 1560, 1473, 1438 (C=C, C=N), 1365 (=C-N), 1219, 1035 (aryl C-O-CH_2). UV-vis: λ_{max}/nm (CH_3CN) 241, 272, 311, 322, 334.

Preparation of Monomer 10

$[Fe(hextpy)_2][PF_6]_2$ (**8**) (1.04 g, 1 mmol), acid complex **5** (1.00 g, 2 mmol), N,N'-dicyclohexylcarbodiimide (0.82 g, 4 mmol), and N,N'-dimethylaminopyridine (0.50 g, 4 mmol) were stirred in DMF (1.5 mL) and dichloromethane (9 mL) under N_2 for 18 h in the dark. The reaction mixture was poured into 1.2 M HCl containing an equimetal molar amount of NH_4PF_6, then extracted into dichloromethane and washed twice with water. The organic extract was dried with $MgSO_4$ and then the solvent was removed *in vacuo*. The resulting precipitate was dissolved in a minimum amount of acetone, added dropwise to diethyl ether, and placed in the freezer. The mixture was filtered and the precipitate was washed with ether to afford a deep purple powder. Yield: 76%. Elemental analysis ($C_{78}H_{70}Cl_2F_{24}Fe_3N_6O_8P_4$): calc. C 45.97%, H 3.46%, N 4.12%; found, C 46.10%, H 3.28%, N 4.45%. NMR data in acetone-d_6: $\delta(^1H)$ 8.85 (s, 4H), 8.79 (m, 4H), 8.23 (d, J = 7.5, 4H), 7.99 (m, 4H), 7.49 (m, 8H), 7.23 (m, 4H), 6.88 (d, J = 5.5, 4H), 6.63 (m, 4H), 5.42 (s, 10H), 4.75 (br s, 4H), 4.45 (t, J = 5.6, 4H), 2.16 (m, 4H), 1.96 (m, 4H), 1.83 (m, 8H); $\delta(^{13}C)$ 169.2, 165.9, 161.9, 159.3, 158.2, 154.6, 139.6, 133.2, 130.9, 129.4, 128.4, 124.8, 121.4, 112.6, 105.5, 88.2, 80.9, 78.6, 71.4, 65.9, 29.6, 29.3, 26.6, 26.5. IR: 1710 (C=O), 1616, 1521, 1500, 1456 (C=C, C=N), 1363 (=C-N), 1274, 1165 (C-O-C ester). UV-vis: λ_{max}/nm (CH_3CN) 246, 268, 315, 367, 506, 557.

Preparation of Monomer 11

Monomer **11** was prepared using a similar procedure as implemented for the synthesis of monomer **10**, combining $[Ni(hex\text{-}tpy)_2][PF_6]_2$ (**9**) (1.05 g, 1 mmol), acid complex **5** (1.00 g, 2 mmol), N,N'-dicyclohexylcarbodiimide (0.82 g, 4 mmol), and N,N'-dimethylaminopyridine (0.50 g, 4 mmol) in DMF (1 mL) and dichloromethane (7 mL) under N_2 for 18 h in the dark. The purification steps remained identical, and the product was isolated as a yellow precipitate. Yield: 25%. Elemental analysis ($C_{78}H_{70}Cl_2F_{24}Fe_2NiN_6O_8P_4$): calc. C 45.91%, H 3.46%, N 4.12 %; found, C 45.66%, H 3.29%, N 3.95%. IR: 1710 (C=O), 1622, 1571, 1537, 1456 (C=C, C=N), 1367 (=C-N), 1244, 1165 (C-O-C ester). UV-vis: λ_{max}/nm (CH_3CN) 243, 271, 311, 323, 334.

Preparation of Polymer 12

Complex **7** (1.26 g, 1 mmol) and $FeCl_2{\cdot}4H_2O$ (0.20 g, 1 mmol) were stirred in a minimum amount of methanol (5 mL) for 18 h. NH_4PF_6 (1.14 g, excess) in 5 mL methanol was added and the reaction mixture was added dropwise to diethyl ether to produce a purple precipitate. The product was isolated *via* vacuum filtration and washed with diethyl ether. NMR data in DMSO-d_6: $\delta(^1H)$ 8.85 (s, 4H), 8.77 (d, 4H), 8.24 (d, J = 8.4, 4H), 7.94 (t, 4H), 7.23 (d, J = 8.4, 4H), 7.18 (m, 4H), 7.14 (m, 4H), 6.48 (s, 4H), 5.01 (s, 5H), 4.58 (s, 4H), 4.46 (t, 4H), 2.08 (m, 4H), 1.88 (m, 4H), 1.76 (m, 8H); $\delta(^{13}C)$ 166.2, 162.6, 160.4, 159.3, 155.8, 153.0, 138.6, 132.2, 130.5, 128.0, 127.5, 123.7, 120.9, 111.5, 77.9, 76.9, 69.8, 65.2, 33.4, 27.5, 25.0, 24.5. IR: 1712 (C=O), 1604, 1502, 1471, 1427 (C=C, C=N), 1363 (=C-N), 1276, 1161 (C-O-C ester). UV-vis: λ_{max}/nm (CH_3CN) 246, 268, 315, 364, 506, 556.

Preparation of Polymer 13

$Ni(CH_3COO)_2{\cdot}4H_2O$ (0.25 g, 1 mmol) was stirred in a minimum amount of methanol for 10 minutes. Complex **7** (1.26 g, 1 mmol) in methanol (7 mL) was added and the mixture was stirred for 18 h. An excess of NH_4PF_6 in methanol (10 mL) was added to the cloudy pink solution, and the flask was put in the freezer for several hours to afford a precipitate. After filtration and washing with methanol and diethyl ether, a fine pink-purple precipitate was collected. IR: 1708 (C=O), 1600, 1566, 1477, 1442 (C=C, C=N), 1365 (=C-N), 1276, 1161 (C-O-C ester). UV-vis: λ_{max}/nm (CH_3CN) 249, 265, 301, 313, 325.

Preparation of Polymer 14

Monomer **10** (2.04 g, 1 mmol), bisphenol A (0.23 g, 1 mmol), and K_2CO_3 (0.97 g, excess) were combined in a minimum amount of DMF (3 mL) under N_2, and stirred for 24 h in the dark. An excess of NH_4PF_6 was added to the reaction mixture, which was then added dropwise to diethyl ether and cooled for 18 h. The resulting solid was filtered and washed with diethyl ether to afford a pink-purple powder. NMR data in acetone-d_6: $\delta(^1H)$ 8.72 (s, 4H), 8.63 (m, 4H), 8.06 (m, 4H), 7.98 (m, 4H), 7.50 (m, 4H), 7.42 (m, 4H), 7.25 (m, 4H), 7.04 (m, 4H), 6.45 (m, 4H), 6.27 (m, 4H), 5.25 (s, 5H), 4.28 (m, 4H), 1.81 (m, 4H), 1.71 (m, 4H), 1.62 (m, 8H), 1.53 (m, 6H). IR: 1710 (C=O), 1598, 1537, 1504, 1471 (C=C, C=N), 1359 (=C-N). UV-vis: λ_{max}/nm (CH_3CN) 241, 267, 315, 556.

Preparation of Polymer 15

Monomer **10** (2.04 g, 1 mmol), hydroquinone (0.11 g, 1 mmol), and K_2CO_3 (0.97 g, excess) were combined in DMF (2.5 mL) and stirred in the dark under N_2 for 48 h. An excess of NH_4PF_6 was added to the flask and the reaction mixture was added dropwise to ether to form a brown/purple oil. The mixture was placed in the freezer for several hours; the diethyl ether was then decanted, the oil was dissolved in a minimum amount of acetone, and the solution was added dropwise to diethyl ether. The resulting precipitate was filtered, washed with diethyl ether, and collected as a dark purple powder. NMR data in acetone-d_6: $\delta(^1H)$ 8.95 (s, 4H), 8.80 (m, 4H), 8.13 (m, 4H), 7.97 (m, 4H), 7.43 (m, 4H), 7.23 (m, 4H), 7.20 (m, 4H), 6.94 (m, 4H), 6.42 (m, 4H), 6.20 (m, 4H), 5.23 (s, 5H), 4.68 (m, 4H), 4.42 (m, 4H), 2.07 (m, 4H), 1.86 (m, 4H), 1.67 (m, 8H). IR: 1708 (C=O), 1612, 1546, 1469 (C=C, C=N), 1365 (=C-N). UV-vis: λ_{max}/nm (CH_3CN) 245, 266, 315, 365, 506, 555.

Computational Methods

Molecular dynamics (MD) simulations were employed to study the conformational flexibility of the organic backbone of complex **7**. To do so, we focused on a truncated model of **7**, whereby the iron moiety was removed along with the cyclopentadienyl ring and counter ion. We will refer to this structure as **7'**. Such an alteration is not expected to significantly affect the flexibility of the ring but obviates the requirement for additional parameters involving the iron center. The MD simulation was carried out using the GROMACS 4.6 package[54-57] combined with the GROMOS 53a6 force field.[58] As GROMACS is primarily designed for bimolecular simulations, parameters for the ligand were developed using the Automated Topology Builder (ATB).[59] Electrostatic interactions were approximated using the Particle Mesh Ewald (PME) method[60] with a coulomb cut-off distance of 1.0 nm, a Fourier spacing of 0.135 nm and an interpolation order of 4. The Lennard-Jones potential[61] was used in the treatment of van der Waals forces while employing a 1.4 nm cut-off distance.

The simulation was carried out in a series of two steps. First, the system underwent a steep descent energy minimization until the maximum force exerted on the atoms converged to within 1000 kJ/mol/nm. The MD simulation was then carried out for a period of 10 ns with a time step of 2 fs. All bonds containing hydrogen atoms were constrained using the LINCS algorithm.[62] The initial velocities for all dynamics simulations were generated from a Maxwell distribution at the appropriate temperature. The temperature (reference temperature of 300 K) and pressure (reference pressure of 1 atm) in the runs were controlled using the velocity-rescale thermostat[63] and Parrinello-Rahmanbarostat, respectively.[64-65] The simulation was performed using the explicit SPC/E[66] water model where the degrees of freedom of the water molecules were constrained using the SETTLE algorithm.[67]

In addition to MD simulations, we also predicted structures and/or harmonic vibrational frequencies of models of compounds **2**, **7'**, and **8** (*vide infra*). For compound **2**, we employed a truncated model whereby the hexanediol moiety was replaced by an OH group, yielding what we will refer to as **2'**. We then optimized this structure using density functional theory. In particular, Becke's three-parameter exchange functional[68] (B3) was employed in conjunction with the correlation functional proposed by Lee, Yang, and Parr[69] (LYP) and the 6-31G* doubly-split-valence Pople basis set. We also predicted the harmonic vibrational frequencies for **2'** both for the purposes of comparison with experimental data and to confirm the nature of the stationary point on the potential energy surface (i.e. a minimum).

In the case of **7'**, our primary focus was to determine the existence and nature of intramolecular interactions between the terminal terpyridine units. We began with the equilibrated MD structure and further optimized the structure using the GROMOS 53a6 force field. To investigate the intramolecular interactions we determined the so-called non-covalent index using the NCI Plot program [70-72] with a promolecular density and graphed these using VMD.[73] Additionally, we calculated the stationary point density of the GROMOS 53a6 optimized structure using the B3LYP/6-31G(d) theoretical method. This density was then used to perform an Atoms in Molecules (AIM) analysis[74-75] with the AIMALL software package[76] to identify and characterize non-covalent interactions by the existence and properties of bond paths between neighbouring terpyridine units.

To afford a comparison of the harmonic vibrational frequencies of **2'** and **7'**, we truncated our GROMOS 53a6 optimized **7'** further by removing all atoms except for the terminal terpyridine units "capped" with hydroxyl groups while holding the spatial positions of the terminal terpyridine units fixed in their fully interacting conformation. We will refer to this truncated interacting terpyridine model as **7i**. We then calculated the B3LYP/6-31G(d) vibrational frequencies of **7i** and compared them to those of **2'**. All vibrational frequencies were scaled by a factor of 0.96.

Finally, we investigated the nature and extent of charge transfer in complex **8** again using an AIM analysis on several structural analogs. We modelled **8** by creating a dimer of **2'** complexed to a central Fe(II) atom. We will refer to this structure as **8'**. We then calculated the AIM atomic charges using AIMALL[76] of **2'**, **8'**, and also **2'** in the exact structural arrangement found in the optimized **8'** complex. The global minimum of **2'** corresponds to a structure having both NCCN dihedral angles equal to 180 degrees. This prevents unfavourable repulsion between the N lone pairs and allows the outer N atoms to interact with neighbouring electron-poor hydrogen atoms from the central heterocycle. To form **8'**, however, the NCCN dihedrals in **2'** reduce to 0 degrees to allow maximum interaction with the positive Fe(II) center. We will refer to this "complexed" geometry of **2'** as **2c'**. We were interested in understanding the charge transfer first from the geometrical rearrangement of **2'** to **2c'** and then from complexation to the Fe(II) center (i.e. **2c'** to **8'**).

All quantum chemical energy calculations, geometry optimizations, and harmonic vibrational frequencies were produced with the Gaussian 09 suite of programs.[77] Cartesian coordinates of our fully optimized **2'**, **7'**, and **8'** complexes are available within the supporting information.

Results and Discussion

Synthesis and Characterization

Many synthetic methods were employed in the preparation of hexanediolterpyridine (hextpy) **2** that utilized the same reagents but different reaction conditions and work-up procedures. The procedure reported by Schubert *et al*. was followed,[50] with several changes to optimize product purity and yield (Scheme 1). A larger molar amount of the nucleophile was used in the reaction (the ratio of hexanediol to tpyCl **1** was increased from 1:1 to 5.5:1), resulting in greater yield, and the reagents were allowed to react for a longer duration (70 °C for up to two days).

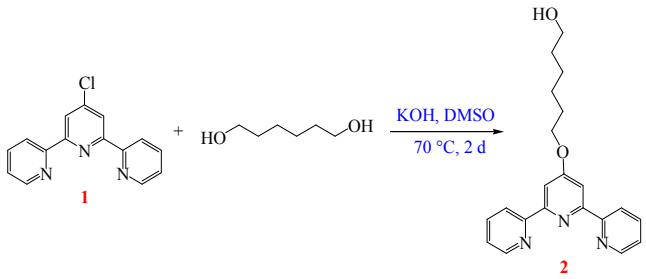

Scheme 1 Synthesis of hextpy **2.**

Novel diacid complex **4** was prepared using a previously reported method.[38] The reaction of dichloro-terminated organoiron complex **3** with 4-hydroxybenzoic acid resulted in the formation of dicarboxylic acid organoiron complex **4**, as shown in Scheme 2. A similar complex already exists within the reported array of organoiron compounds, but with either a single carboxylic acid group or two aldehyde moieties.[38,78] Diacid complex **4** was therefore prepared to later afford an organoiron-containing monomer with two terminal terpyridine moieties through an esterification reaction.

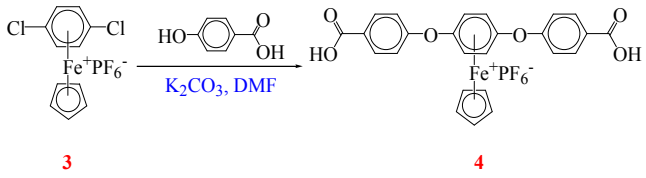

Scheme 2 Synthesis of diacid complex **4.**

In the ^{1}H NMR spectrum of complex **4**, the Cp singlet appears at 5.43 ppm, slightly downfield from its resonance in complex **3** at 5.48 ppm, confirming substitution. The aryl protons appear as a singlet at 6.59 ppm, further supporting successful disubstitution, as monosubstitution would result in two doublets. The proton signals of the non-complexedarene show doublets at 8.17 and 7.43 ppm. No peaks representing either starting material appear in the spectrum, confirming completion of the reaction.

A typical carbonyl stretch of a carboxylic acid group on an aromatic ring appears at 1697 cm^{-1} in the IR spectrum of diacid complex **4**, while the C-O stretching band occurs at 1288 cm^{-1}. The stretches at 1232 cm^{-1} and 1128 cm^{-1} demonstrate the stretching of the diaryl ether C-O-C bonds, supporting the formation of the ether. The UV-vis spectrum shows one band at 246 nm, representing the $\pi \rightarrow \pi^*$ transition of the aromatic rings.

The first organoiron-containing terpyridine compound, **6**, was prepared *via* a condensation reaction with acid complex **5** and hextpy **2** (Scheme 3).[38,49]

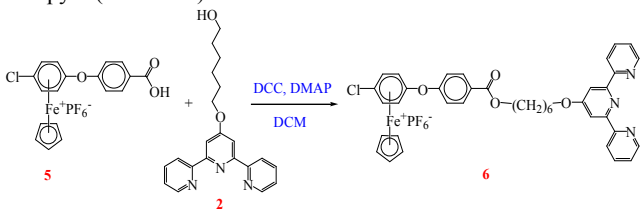

Scheme 3 Synthesis of organoiron-containing terpyridine **6**.

The IR spectrum of complex **6** shows a shift in the C=O stretch to a higher wavenumber (1710 cm^{-1}) than the starting material. Aryl ester C=O stretches occur at a lower frequency than those of aliphatic esters due to the increased conjugation. The carbon-carbon and carbon-nitrogen double bond stretches of the terpyridine moiety are present in the region from 1400-1650 cm^{-1}, and the =C-N stretch is found at 1357 cm^{-1}. The C-O-C stretches of the ester functionality appears at 1278 cm^{-1} and 1161 cm^{-1}, confirming a successful reaction.

The gradient heteronuclear single quantum coherence (gHSQC) NMR spectrum shows that the signal at 4.33 ppm represents both the methylene protons adjacent to the ester, shifted downfield from 4.24 ppm in hextpy **2**, as well as the methylene protons adjacent to the oxygen bonded to the terpyridine.

Diacid **4** was reacted with hextpy **2** in a Steglich esterification reaction using the same conditions as in the preparation of complex **6** to afford complex **7** with two terminal terpyridine groups as shown in Scheme 4.

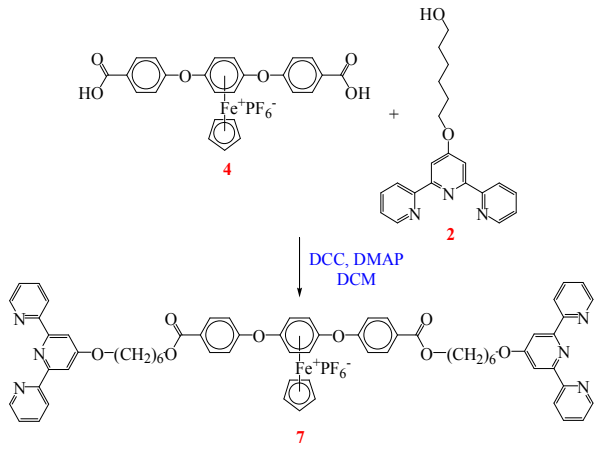

Scheme 4 Synthesis of organoiron-containing terpyridine **7.**

The ^{1}H NMR of complex **7** shows the product peaks, as well as the presence of some diacid starting material, in a ratio of 5:1. The ester groups are slightly less deshielding than the acid groups of starting organoiron complex **4**, causing a small shift upfield in the resonances of the cyclopentadienyl protons and the complexed and non-complexed aryl hydrogens. As in monosubstituted complex **6**, the multiplet at 4.32 ppm represents both the methylene protons next to the ester group and those adjacent to the oxygen bonded to the terpyridine group, as confirmed by gHSQC data. As in monosubstituted complex **6**, complex **7** with diester functionalities shows similar IR stretches to confirm the successful esterification reaction. The C=O stretch shifts from 1697 cm^{-1} in starting material diacid complex **4** to 1710 cm^{-1}, while the C-O-C ester stretches occur at 1271 cm^{-1} and 1165 cm^{-1}. The terpyridine C=C and C=N stretching frequencies appear in the 1400-1650 cm^{-1} region, shifting to slightly higher wavenumbers than in starting material hextpy **2**. The =C-N stretch follows the same trend, shifting approximately 20 cm^{-1} higher in frequency to 1346 cm^{-1} than its equivalent in hextpy **2**. This shift to lower energy is likely a result of intramolecular interactions; the hexyl chains are fairly flexible, allowing the terpyridine units to interact with nearby terpyridine groups or the second terminal terpyridine group within the same molecule. This can be readily demonstrated using computational techniques. We've performed molecular dynamics simulations to understand the flexibility of the hexyl chains and quantum chemical calculations to demonstrate that intramolecular interactions are present and elucidate their effect on the vibrational frequencies.

A molecular dynamics simulation was performed on **7'** according to the procedure described in the Computational Methods in order to determine an average structure for the ligand. This average structure was obtained by analyzing the root mean square deviation (RMSD) from the initial structure. The average was calculated from the final 2000 ps of the simulation based on an observed equilibrium in the plot of the RMSD (see supporting information). As the average structures computed from GROMACS are generally crude, a subsequent energy minimization was carried out using the GROMOS 53a6 force field to obtain the final geometry (Cartesian coordinates available in the supporting information). The geometry of compound **7'** is characterized by a folding pattern that allows the terminal terpyridine units to readily interact. This is illustrated in Fig. 1 (left), which depicts the interaction surface for these units as predicted by a promolecular density using NCI Plot.[71] This technique determines and visualizes Van der Waals interactions by calculating points of low reduced electron density gradient. The isosurface shown in green is strong evidence for weak interactions that are primarily found near the N atoms.

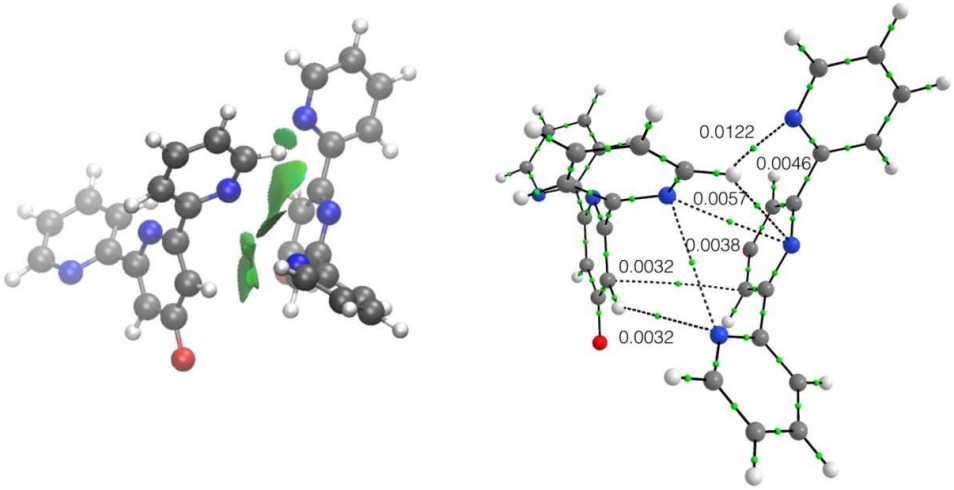

Fig. 1 The interaction surface as predicted by a promolecular density using NCI Plot[71] (shown in green) for the terminal terpyridine units in **7'** (left) and the molecular graph with selected bond critical point densities indicated (right). Both are depicted in a similar orientation. For clarity, all atoms other than the terminal terpyridines have been removed. Non-bonded interactions are plotted using dashed lines and selected bond critical point densities are given in atomic units. Carbon atoms are illustrated in grey, nitrogen atoms are indicated in blue, oxygen atoms are indicated in red and hydrogen atoms are indicated in white. Bond critical points are indicated as small green spheres.

Cite this: DOI: 10.1039/c0xx00000x

www.rsc.org/xxxxxx

ARTICLE TYPE

Additionally, we investigated the topology of the electron density using Bader's Quantum Theory of Atoms in Molecules (AIM) to understand the extent of the interaction between these terminal terpyridine groups. As shown in Fig. 1 (right), there are several bond paths predicted by the B3LYP/6-31G(d) density that indicate significant interaction (shown as dashed lines). These are paths of maximum electron density between two atoms and are strong indicators for interatomic interactions. The bond critical point densities are illustrated in atomic units and are all of appropriate magnitude to affect properties such as the terpyridine normal modes.

Indeed, in excellent agreement with the experimental IR spectra, we find that the harmonic vibrational frequencies of **2'** are consistently lower in energy than the corresponding modes of the truncated model of **7i** by about 20 or more wavenumbers (see supporting information).

The UV-vis spectra of complexes **6** and **7** are very similar, showing matching absorbance bands in the 220-360 nm range (Fig. 2). The peaks at 245 nm and 275 nm represent the $\pi \rightarrow \pi^*$ transitions of the terpyridyl groups. The absorbance band at 245 nm also overlaps with the peak representative of the $\pi \rightarrow \pi^*$ transition of the aromatic rings of the cationic iron ester moiety, which appears at 246 nm in the UV-vis spectra of starting materials monoacid **5** and diacid **4**.

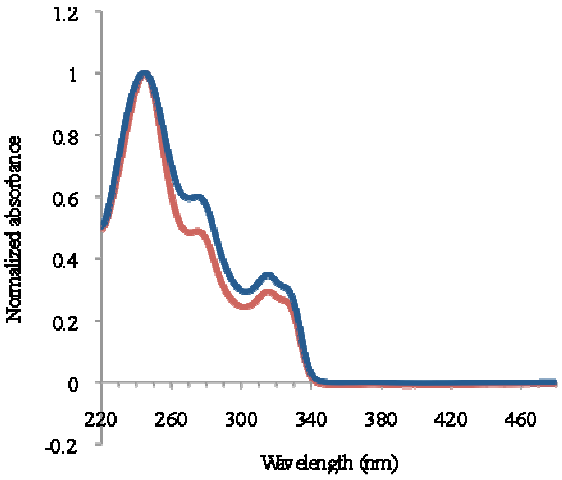

Fig. 2 Comparison of UV-visible spectra of complex **6** (red) and complex **7** (blue) in the region of 220-480 nm.

Two novel metal-chelated complexes of hextpy **2** were prepared to demonstrate a small portion of the range of possible metal-organic frameworks containing terpyridines. The metal-chelated complexes employed either iron(II) or nickel(II); iron(II) was used for most polymerization reactions due to the facile and efficient reaction conditions, minimal purification required, and diamagnetic properties.

The iron(II)-chelated terpyridine complex **8** was synthesized by a modification of a published procedure (Scheme 5).[79] The iron-chelated product was a deep purple powder, the expected colour of iron-terpyridine complexes.[35,80]

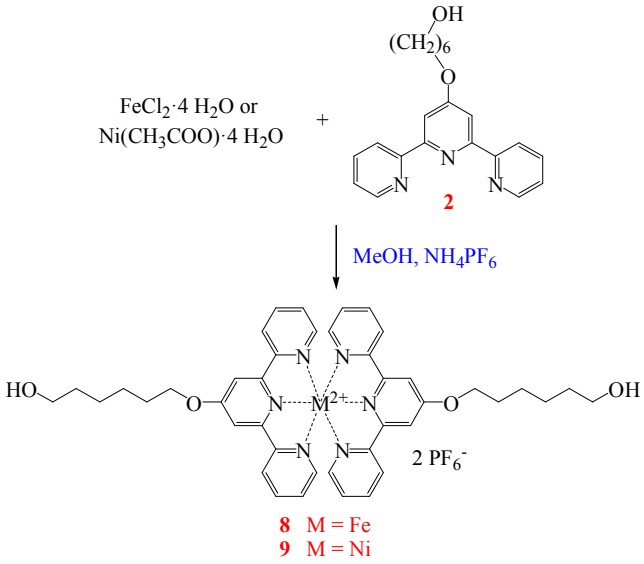

Scheme 5 Synthesis of $[M(hextpy)_2][PF_6]_2$ {M = Fe (**8**) and M= Ni (**9**)}.

The ^{1}H NMR spectrum of complex **8** in DMSO-d_6 showed significant shifts in all of the proton environments of the terpyridine moieties in response to chelation to iron (Fig.. 3).

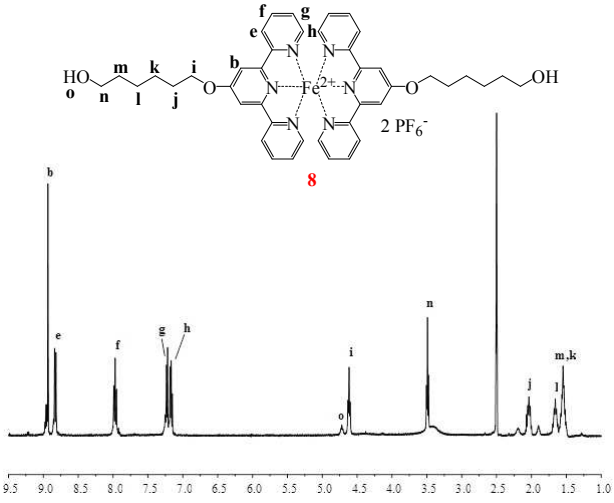

Fig. 3 ^{1}H NMR spectrum of iron-chelated complex **8** in DMSO-d_6.

The singlet representing the 3′,5′-protons (H_b) shifts downfield from 7.97 ppm to 8.93 ppm, while the 3,3″-protons (H_e) shift downfield from 8.60 ppm to 8.83 ppm. The 4,4″-proton (H_f) resonance shows little variation as a triplet of doublets at 7.97 ppm, while both the 5,5″- and 6,6″-protons (H_g and H_h) move upfield to 7.17 and 7.23 ppm, respectively. These upfield shifts are in direct response to chelation to the iron(II) center, which accepts electrons from the terpyridine nitrogens. The lone pairs on the nitrogens contribute less to the electron density in the pyridyl rings, decreasing the electron density in the aromatic system, and therefore shielding the protons nearest the iron moiety. The upfield shifting of protons H_h can be explained by their position in the shielding region above a pyridine ring of the other ligand.[81] The shifting of protons H_b depends upon the nature of the substituent, but these hydrogens often resonate near protons H_e. The methylene protons next to the ether linkage (H_i) shift slightly downfield, appearing at 4.62 ppm. A broad triplet is present at 4.72 ppm, indicating H_o of the intact hydroxyl group.

The downfield shift of the methylene protons is due to the metal center pulling electron density away from the terpyridine moiety as a whole, thus causing the aromatic terpyridyl system to deshield the surrounding proton environments. This is demonstrated in Fig. 4, in which the change in atomic charges (as predicted by AIM theory) is shown for **2'** as it undergoes geometrical rearrangement to **2c'** and then complexes with Fe(II) to form **8'**.

Iron(II) and nickel(II) complexes of 4′-hexyl alcohol-2,2′:6′,2″-terpyridine were prepared by reaction of the terpyridine ligand with iron(II) chloride or nickel(II) acetate, respectively. ^{1}H NMR spectroscopy confirmed that chelation to the metal center caused a definitive upfield shift in the terpyridyl protons closest to the metal, while the terpyridine protons in the 3′,5′-position shifted downfield significantly. UV-visible spectroscopy confirmed characteristic metal-ligand charge transfer bands for the iron(II) complexes (~556 nm) as well. A new diacid-functionalized organoiron complex was synthesized to act as a spacer in a terpyridine monomer. This diacid complex was reacted with hexanediol-functionalized terpyridine in a Steglich esterification to afford a monomer containing two terminal terpyridine units. Similarly, the hexanediol-functionalized terpyridine was also reacted with a monoacid-containing cationic iron complex, resulting in a complex that could then be polymerized through either coordination polymerization or condensation polymerization. Four new organoiron-containing coordination polymers were prepared: three included iron(II)-chelated terpyridine units and one contained terpyridine-nickel(II) complexation. The thermal properties of the iron(II) polymers were studied by thermogravimetric analysis and differential scanning calorimetry. The incorporation of the coordination complex into the backbone of the polymer resulted in lower glass transition temperatures but higher thermal stability than their organoiron polymer analogues free of coordination bonds.

As can be seen in Fig. 4, the majority of charge transfer occurs between the N and Fe atoms, as expected. Upon complexation, the N atoms of each **2c'** collectively gain 0.55 e of charge, while the Fe center gains 0.62 e (0.31 e coming from each **2c'** molecule). This increase in electron density comes at the expense of the remaining atoms in the aromatic ring structures, with the exception of carbons 2, 8, and 10 (and their symmetrically equivalent analogues). These centers appear to be the shuttle through which the density transfers and thus have relatively little net change in atomic charge. The positive increase in charge on the N atoms upon geometrical rearrangement is primarily due to the repulsion between N lone pairs, forcing electron density back into the ring structure of the terpyridine moiety.

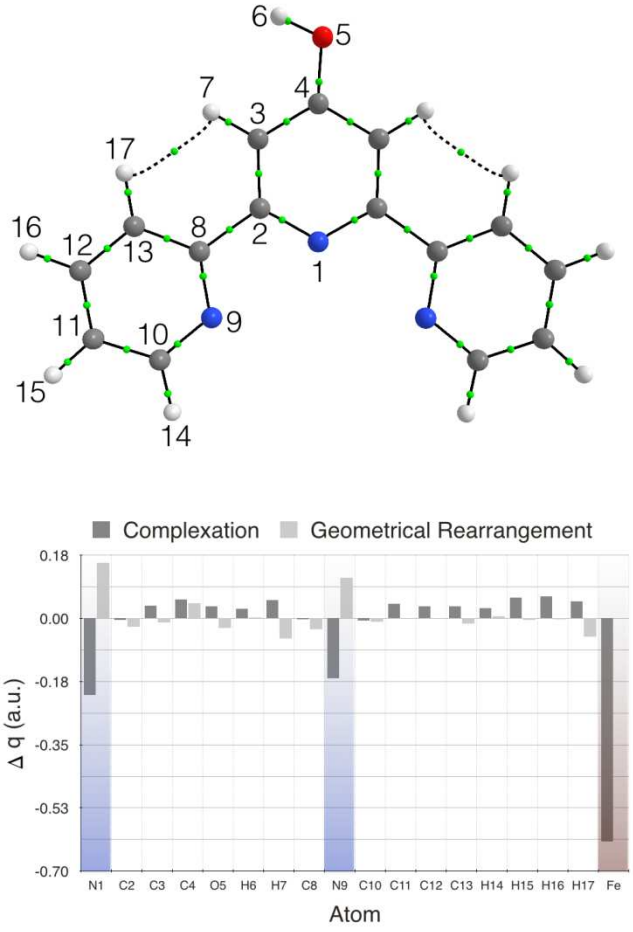

Fig. 4 Molecular graph of **2c'** (top) with all unique atoms numbered and bond critical points indicated. The chart (bottom) shows the change in atomic charge (Δq) of each atom from the geometrical rearrangement of **2'** to **2c'** and then complexation to the Fe(II) center from **8'**. The Fe and N atoms are highlighted in brown and blue, respectively.

$[Ni(hex\text{-}tpy)_2][PF_6]_2$ (**9**) was prepared using a modified procedure.[82] Due to its paramagnetic nature, the ^{1}H NMR spectrum of the complex did not appear useful. However, according to a similar reaction reported by Constable and coworkers using cobalt(II), signals outside of the studied 0-14 ppm range would have provided information regarding the terpyridyl protons.[83]

Acid complex **5** was reacted with metal-chelated terpyridine complexes **8** or **9** to form chloro-terminated monomers **10** and **11** for condensation polymerization (Scheme 6).[38,78,84-88] Monomer

10 was isolated as a purple powder, while monomer **11** was a yellow precipitate.

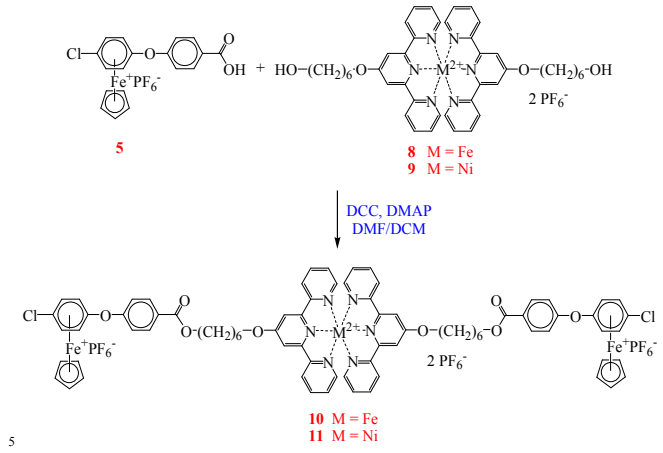

Scheme 6 Synthesis of monomers **10** and **11.**

The ^{1}H NMR spectrum of monomer **10** confirms successful synthesis by the downfield shift in the methylene protons closest to the hydroxyl group of starting material **8**, shifting from 3.62 ppm to 4.45 ppm upon esterification. This shift is a direct result of the greater deshielding effect of the ester group compared to the hydroxyl group of starting material **8**.

Similarly, the peaks representing the aromatic protons of the former iron complex are slightly affected by the esterification reaction, with *ortho* and *meta* protons of benzoic acid shifting slightly downfield (~0.03 ppm) compared to the acid complex starting material due to their proximity to the deshielding ester moiety. The *ortho* and *meta* protons of the C_6H_4ClO moiety shift slightly upfield, by 0.03 ppm, while the Cp protons shift from 5.45 ppm in acid complex **5** to 5.42 ppm in monomer **10** as expected from similar esterification reactions using cationic iron moieties.[38,49,87-90]

IR spectroscopy supports the formation of monomer **10**. The ester C=O stretch appeared at 1710 cm^{-1}, mirroring the same carbonyl stretch in similarly functionalized complex **6**. The terpyridine C=C and C=N stretching frequencies were shifted to the left, as expected upon chelation to iron to 1616 cm^{-1}, 1521 cm^{-1}, 1500 cm^{-1}, and 1456 cm^{-1}. Similarly, the =C-N stretch shifted to a slightly higher wavenumber at 1363 cm^{-1}, and C-O-C ester stretches were present at 1274 cm^{-1} and 1165 cm^{-1}, confirming successful esterification. The terpyridyl stretches of nickel(II) monomer **11** matched closely to these values as well.

The UV-vis absorbance spectrum of monomer **10** is very similar to that of starting material **8** (Fig. 5). The $\pi \rightarrow \pi^*$ transitions of the terpyridine groups appear at 246 nm and 268 nm, while the $\pi \rightarrow \pi^*$ transition affected by the iron(II) center remains at 315 nm. The transition at 246 nm is more intense in monomer **10** due to the overlap of the $\pi \rightarrow \pi^*$ transitions of the terpyridine moieties and the aromatic rings of the cationic iron complex. A broad MLCT band is present at 557 nm, with small shoulder peaks at 367 nm and 506 nm, which are indicative of metal-centered d-d transitions. Similarly, the UV-vis spectrum of monomer **11** is almost identical to its starting material, complex **9**, in the positioning of each absorbance band. The ligand-centered $\pi \rightarrow \pi^*$ transitions appear at 243 nm and 271 nm, with those affected by the chelation to the nickel(II) center appearing less intensely at 311 nm and 323 nm.[16,19] The band at 334 nm is most likely a result of a nickel-centered d-d transition.[91]

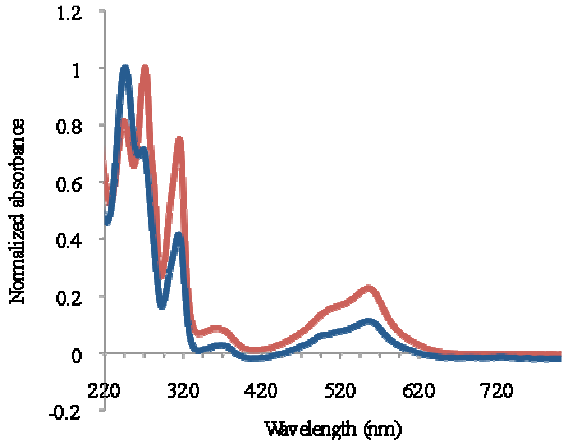

Fig. 5 Comparison of UV-vis spectra of complex **8** (red) and monomer **10** (blue).

Monomer **7** was prepared for the purpose of coordination polymerization by the reaction of the terminal terpyridine groups with a metal salt. Polymer **12** was formed when monomer **7** and iron(II) chloride were combined in a minimum amount of methanol for 18 hours (Scheme 7). Upon addition of ammonium hexafluorophosphate and precipitation in diethyl ether, the product was afforded as a purple precipitate.

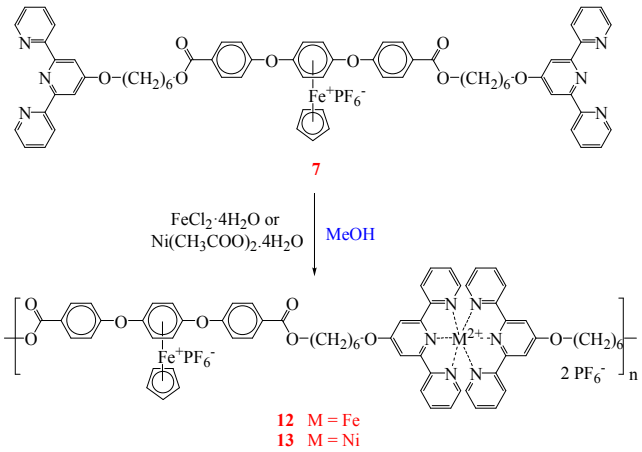

Scheme 7 Synthesis of iron(II) and nickel(II) coordination polymers **12** and **13**, respectively.

NMR spectroscopy confirmed the successful coordination of terpyridine to iron(II) or nickel(II) through the characteristic shifts of the terpyridyl hydrogen environments. In addition to the distinctive shifts of the proton signals upon chelation to iron, all

resonances in the ^{1}H NMR spectrum of polymer **12** were broadened, a known attribute of polymeric materials. Nearly all other proton resonances of polymer **12** shift downfield from their chemical shifts in starting material **7** upon polymerization. For example, the methylene protons beside the ester functionality appear at 4.46 ppm, downfield from 4.32 ppm, while the methylene protons at the other end of the hexyl chain, located next to the ether linkage, shift from 4.32 ppm to 4.58 ppm. The Cp protons, however, shift upfield from 5.26 ppm in monomer **7** to 5.01 ppm in polymer **12**, as is expected in polymers containing cationic iron moieties.[49,78,85-89]

The UV-visible spectrum of polymer **12** is nearly identical to that of monomer **10** as expected, since the structure of the polymer is very similar to that of its monomer. The $\pi \rightarrow \pi^*$ transitions of the terpyridine groups still appear at 246 nm and 268 nm, while the $\pi \rightarrow \pi^*$ transition affected by the iron(II) center remains at 315 nm. Shoulder peaks at 364 nm and 506 nm represent the d-d transitions localized at the iron center, while the metal-to-ligand charge transfer band appears at 556 nm.

The infrared spectrum of polymer **12** aided in confirming chelation of the terpyridine end groups to iron(II) due to the shift to higher wave numbers of the C=C and C=N terpyridyl stretching frequencies in the range of 1420-1650 cm^{-1}. Also, the =C-N stretch shifted from 1346 cm^{-1} in free ligand complex **7** to 1363 cm^{-1} due to the increase in double bond character upon chelation to the metal center, which is the case for most metal-terpyridine complexes.[92]

Monomer **7** was also reacted with nickel(II) acetate in methanol for 18 hours to produce nickel(II)-containing coordination polymer **13** as a pink-purple powder (Scheme 7). IR spectroscopy provides strong evidence that the polymer was successfully formed. The frequencies of the terpyridine-based stretches and the ester functionalities appear at very similar wave numbers as their corresponding peaks in complex **9**, [Ni(hex-tpy)$_2$][PF$_6$]$_2$. The C=C and C=N peaks appear at 1600 cm^{-1}, 1566 cm^{-1}, 1477 cm^{-1}, and 1442 cm^{-1}, and the C-O-C stretches of the ester groups mirror those found in complex **9**, appearing at 1276 cm^{-1} and 1161 cm^{-1}. The =C-N stretching frequency shifts ~20 cm^{-1} to the left to 1365 cm^{-1} to confirm chelation to the metal center. The most noticeable new stretch is the carbonyl stretch of the ester functionality at 1708 cm^{-1}, shifted to a slightly lower wave number than in complex **9**.

The ligand-centered $\pi \rightarrow \pi^*$ transitions of the terpyridyl moieties and the aromatic backbone of polymer **13** appear at 249 and 265 nm, respectively, in the UV-visible spectrum. The $\pi \rightarrow \pi^*$ transitions influenced by the chelation to nickel appear red-shifted at 301, 313, and 325 nm.

Monomer **10** was reacted with a spacer, either bisphenol A or hydroquinone, for 24 hours in darkness to give coordination polymers **14** and **15** (Scheme 8). The ^{1}H NMR spectra of polymers **14** and **15** show broad resonances, indicative of polymerization. In both spectra, the Cp signal appears at approximately 5.23 ppm, shifted upfield from 5.42 ppm in monomer **10**, confirming successful polymerization.

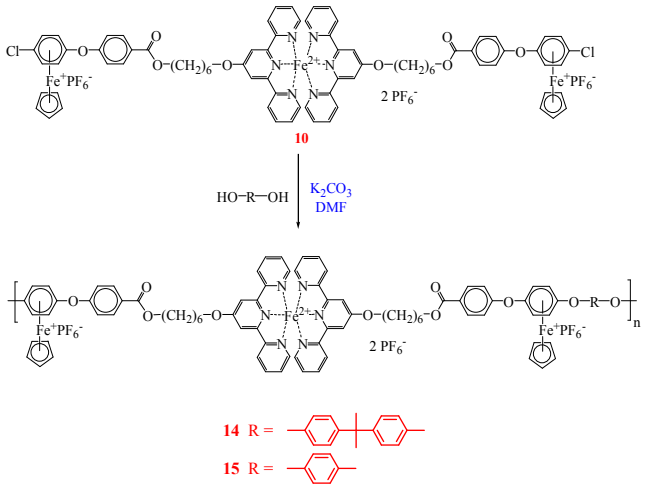

Scheme 8 Synthesis of Fe(II) coordination polymers **14** (bisphenol A spacer) and **15** (hydroquinone spacer).

The ^{1}H NMR spectra of polymer **15** and monomer **10**, shown as an example, provided evidence of polymerization (Fig. 6). The shifts of the complexed aryl protons shows the substitution of the chloro group by the phenolic spacer, and the appearance of the aromatic protons of the hydroquinone moiety at 6.92 ppm further support the successful synthesis of polymer **15**.

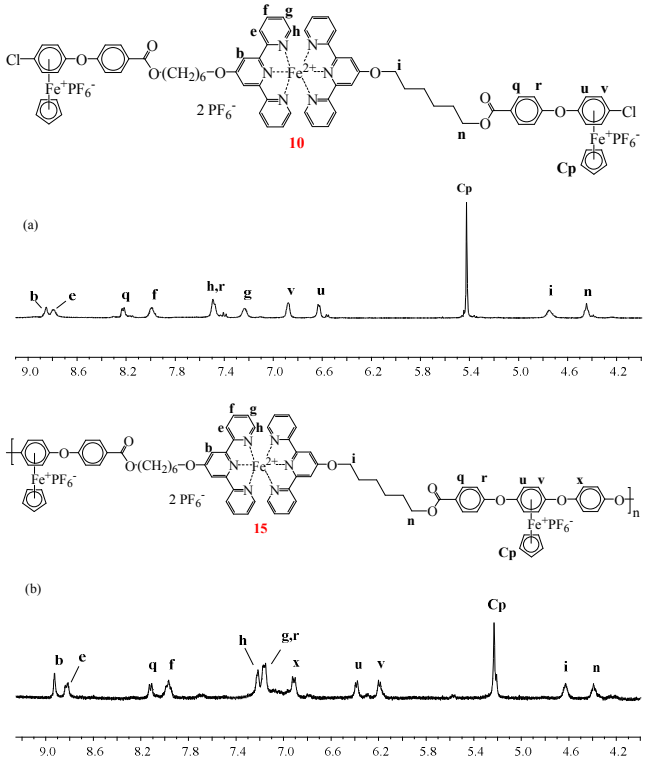

Fig. 6 (a) ^{1}H NMR spectrum of monomer **10** in DMSO-d_6 and (b) ^{1}H NMR spectrum of polymer **15**, with hydroquinone spacer, in acetone-d_6.

Given the similarity in their overall structures, the UV-visible spectra of both polymers **14** and **15** appear very similar to that of monomer **10**, including the $\pi \rightarrow \pi^*$ transitions of the terpyridine groups below 300 nm, with those affected by the iron center at 315 nm, and the broad MLCT band around 555 nm.

Thermogravimetric analysis (TGA) was performed on terpyridine-containing iron(II) coordination polymers **12**, **14**, and **15**, as summarized in Table 1. The thermal degradations are similar across all three polymers, most likely due to their similar structures, and therefore polymer **12** is discussed as an example.

Table 1 Summary of TGA results of iron-containing polymers **12**, **14**, and **15.**

Compound	Step 1	Step 2	Step 3	Step 4
	T_d (°C) (% wt)	T_d (°C) (% wt)	T_d (°C) (% wt)	T_d (°C) (% wt)
12	159.81 (5.4%)	219.06 (22.3%)	388.99 (27.5%)	523.76 (3.8%)
14	161.13 (7.6%)	190.30 (30.2%)	345.76 (23.7%)	525.40 (3.2%)
15	151.16 (6.3%)	206.41 (31.8%)	343.47 (31.8%)	550.67 (5.4%)

The thermogram of polymer **12** indicates thermal degradation occurred in four steps (Fig. 7).

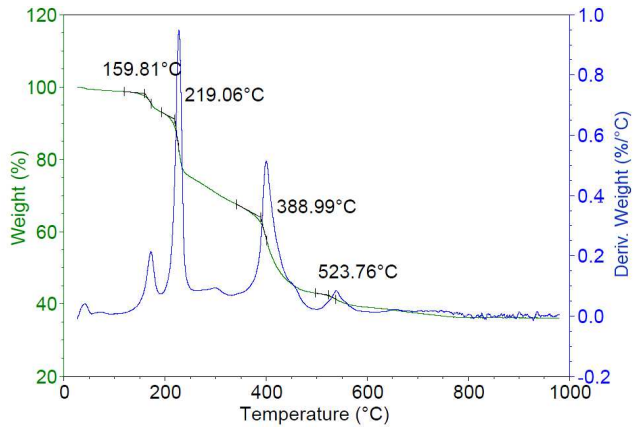

Fig. 7 TGA of polymer **12.**

The weight loss of 22.3% with thermal stability up to 219.06 °C can be attributed to the decoordination of the cyclopentadienyliron(II) moiety, which has been previously shown to decompose between 180-240 °C.[38,49,78,84-89,93] The third decomposition step at 388.99 °C (weight loss of 27.5%) is the degradation of the aromatic backbone of the polymer. This loss occurs at a higher temperature due to the higher bond dissociation energies of aryl bonds. The final weight loss of 3.8% at 523.76 °C correlates to the decomposition of the Fe-N bonding interaction due to its higher bond dissociation energy.[94-96] All three polymers have final decomposition temperatures significantly higher than those observed in organoiron polymers previously [38,49,84,88] due to the presence of the Fe-N coordination bond.

The thermal stability of polymers **12**, **14**, and **15** was further assessed by performing differential scanning calorimetry (DSC). This study provides a glass transition temperature (T_g) for a polymeric material, which is a function of chain flexibility. Below T_g, an amorphous polymer exists in a rigid and glassy state; above T_g, it transitions to its rubbery and pliable state. The ease of movement of a polymer chain determines whether the glass transition temperature will be high or low: a polymer chain that can move around fairly easily will have a very low T_g, while one that is more confined will have a higher T_g.[97-99] The glass transition temperature for polymer **12** is -21.17 °C (Fig.8), while its nickel(II) analogue has a T_g of -20.10 °C. The T_g values for polymers **14** and **15** are -21.50 °C and -21.92 °C, respectively, suggesting that such structurally similar polymer backbones will have comparable glass transition temperatures, as polymer **14** contains bisphenol moieties while polymer **15** contains hydroquinone groups.

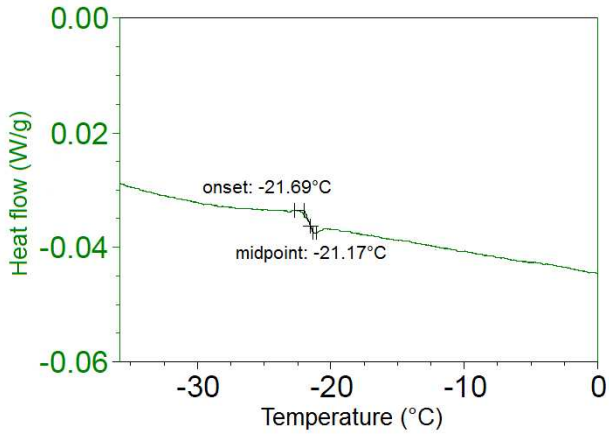

Fig. 8 DSC curve of polymer **12** (T_g = -21.17 °C).

These values are much lower than the glass transition temperatures for other linear polymers containing organoiron moieties in their backbones previously published,[38,49,85] confirming that the presence of the coordination bond lowers the T_g of the polymer while making it more thermally stable with higher decomposition temperatures.

Conclusions

Iron(II) and nickel(II) complexes of 4′-hexyl alcohol-2,2′:6′,2″-terpyridine were prepared by reaction of the terpyridine ligand with iron(II) chloride or nickel(II) acetate, respectively. ^{1}H NMR spectroscopy confirmed that chelation to the metal center caused a definitive upfield shift in the terpyridyl protons closest to the metal, while the terpyridine protons in the 3′,5′-position shifted downfield significantly. UV-vis spectroscopy confirmed characteristic metal-ligand charge transfer bands for the iron(II) complexes (~556 nm) as well. A new diacid-functionalized organoiron complex was synthesized to act as a spacer in a terpyridine monomer. This diacid complex was reacted with hexanediol-functionalized terpyridine in a Steglich esterification to afford a monomer containing two terminal terpyridine units. Similarly, the hexanediol-functionalized terpyridine was also reacted with a monoacid-containing cationic iron complex, resulting in a complex that could then be polymerized through either coordination or condensation polymerization. Four new organoiron-containing coordination polymers were prepared:

three included iron(II)-chelated terpyridine units and one contained terpyridine-nickel(II) complexation. The thermal properties of the iron(II) polymers were studied by thermogravimetric analysis and differential scanning calorimetry. Several properties of these compounds were also characterized via computational simulation. The incorporation of the coordination complex into the backbone of the polymer resulted in lower glass transition temperatures but higher thermal stability than their organoiron polymer analogues free of coordination bonds.

Acknowledgements

Financial support provided by the Natural Sciences and Engineering Research Council of Canada is gratefully acknowledged. Assistance of Mr. Michael Cowper with TGA and DSC analysis is appreciated.

Notes and references

[a]*Department of Chemistry, University of Prince Edward Island, 550 University Avenue, Charlottetown, Prince Edward Island, Canada, C1A 4P3, Fax: (902) 628-4311; E-mail: abdelaziz@upei.ca*
[b]*Department of Chemistry, University of British Columbia, Kelowna, British Columbia, Canada, VIV 1V7*
[c]*Faculty of Chemistry, K.N. Toosi University of Technology, P.O. Box 16315-1618, Tehran 15418, Iran*
† Electronic Supplementary Information (ESI) available: [details of any supplementary information available should be included here]. See DOI: 10.1039/b000000x/

1 B. Moulton and M. J. Zaworotko, *Curr. Opin. Solid State Mater. Sci*., 2002, **6**, 117.
2 A. S. Abd-El-Aziz, J. L. Pilfold, I. Kucukkaya and M. S. Vandel, in Encyclopedia of Polymer Science and Technology, ed. H. F. Mark, John Wiley & Sons, Chichester, 2012.
3 A. S. Abd-El-Aziz and E. A. Strohm, *Polymer*, 2012, **53**, 4879.
4 A. Wild, A. Winter, F. Schlütter and U. S. Schubert, *Chem. Soc. Rev*., 2011, **40**, 1459.
5 U. S. Schubert, A. Winter and G. R. Newkome, Terpyridine-Based Materials: For Catalytic, Optoelectronic and Life Science Applications, John Wiley & Sons, Chichester, 2011.
6 A. S. Abd-El-Aziz, P. O. Shipman, B. N. Boden and W. S. McNeil, *Prog. Polym. Sci*., 2010, **35**, 714.
7 J. E. Beves, E. C. Constable, C. E. Housecroft, M. Neuburger and S. Schaffner, *Inorg. Chem.Commun.*, 2009, **12**, 898.
8 U. S. Schubert, H. Hofmeier and G. R. Newkome, *Modern Terpyridine Chemistry*, John Wiley & Sons, Chichester, 2006.
9 J. Chambers, B. Eaves, D. Parker, R. Claxton, P. S. Ray and S. J. Slattery, *Inorg. Chim. Acta*, 2006, **359**, 2400.
10 P. R. Andres, R. Lunkwitz, G. R. Pabst, K. Böhn, D. Wouters, S. Schmatloch and U. S. Schubert, *Eur. J. Org. Chem*., 2003, 3769.
11 B. G. G. Lohmeijer and U. S. Schubert, *J. Polym. Sci. Part A*, 2003, **41**, 1413.
12 U. S. Schubert and C. Eschbaumer, *Angew. Chem. Int. Ed.*, 2002, **41**, 2892.
13 G. F. Swiegers and T. J. Malefetse, *Chem. Rev.*, 2000, **100**, 3483.
14 S. D. Cummings, *Coord. Chem. Rev.*, 2009, **253**, 449.
15 A. M. W. Cargill Thompson, *Coord. Chem. Rev*., 1997, **160**, 1.
16 M. Chiper, M. A. R. Meier, J. M. Kranenburg and U. S. Schubert, *Macromol. Chem. Phys.*, 2007, **208**, 679.
17 M. Heller and U. S. Schubert, *Eur. J. Org. Chem*., 2003, 947.
18 U. S. Schubert, S. Schmatloch and A. A. Precup, *Des.Monomers Polym*., 2002, **5**, 211.
19 U. S. Schubert, C. Eschbaumer, P. Andres, H. Hofmeirer, C. H. Weidl, E. Herdtweck, E. Dulkeith, A. Morteani, N. E. Hecker and J. Feldmann, *Synth. Met*., 2001, **121**, 1249.
20 C. Bazzicalupi, A. Bencini, A. Bianchi, A. Danesi, E. Faggi, C. Giorgi, S. Santarelli and B. Valtancoli, *Coord. Chem. Rev*., 2008, **252**, 1052.
21 P. Lainé, F. Bedioui, P. Ochsenbein, V. Marvaud, M. Bonin and E. Amouyal, *J. Am. Chem.Soc*., 2002, **124**, 1364.
22 P. R. Ashton, R. Ballardini, V. Balzani, E. C. Constable, A. Credi, O. Kocian, S. J. Langford, J. A. Preece, L. Prodi, E. R. Schofield, N. Spencer, J. F. Stoddart and S. Wenger, *Chem. Eur. J*., 1998, **4**, 2413.
23 A. El-Ghayoury and R. Ziessel, *Tetrahedron Lett*., 1997, **38**, 2471.
24 A. Harriman and R. Ziessel, *J. Chem. Soc. Chem. Commun*., 1996, 1707.
25 G. Pickaert and R. Ziessel, *Tetrahedron Lett*., 1998, **39**, 3497.
26 T. E. Janini, J. L. Fattore and D. L. Mohler, *J. Organomet. Chem*., 1999, **578**, 260.
27 U. Sampath, W. C. Putnam, T. A. Osiek, S. Touami, J. Xie, D. Cohen, A. Cagnolini, P. Droege, D. Klug, C. L. Barnes, A. Modak, K. Bashkin and S. S. Jurisson, *J. Chem. Soc.Dalton Trans*., 1999, 2049.
28 E. C. Constable, A. J. Edwards, M. D. Marcos, P. R. Raithby, R. Martínez-Máñez and M. R. L. Tendero, *Inorg. Chim. Acta*, 1994, **224**, 11.
29 G. Albano, V. Balzani, E. C. Constable, M. Maestri and D. R. Smith, *Inorg. Chim. Acta*, 1998, **277**, 225.
30 E. C. Constable, R. Handel, C. E. Housecroft, M. Neuburger, E. R. Schofield and M. Zehnder, *Polyhedron*, 2004, **23**, 135.
31 E. Figgemeier, V. Aranyos, E. C. Constable, R. W. Handel, C. E. Housecroft, C. Risinger, A. Hagfeldt and E. Mukhtar, *Inorg. Chem. Commun*., 2004, **7**, 117.
32 E. C. Constable, M. Neuburger, D. R. Smith and M. Zehnder, *Inorg. Chim. Acta*, 1998, **275-276**, 359.
33 E. C. Constable, B. M. Kariuki and A. Mahmood, *Polyhedron*, 2003, **22**, 687.
34 D. Armspach, E. C. Constable, F. Diederich, C. E. Housecroft and J.-F. Nierengarten, *Chem. Eur. J*., 1998, **4**, 723.
35 S. Schmatloch and U. S. Schubert, *Macromol. Symp*., 2003, **199**, 483.
36 A. El-Ghayoury, A. P. H. J. Schenning and E. W. Meijer, *J. Polym. Sci. Part A: Polym. Chem.*, 2002, **40**, 4020.
37 A. S. Abd-El-Aziz, C. R. de Denus, M. J. Zaworotko and L. R. MacGillivray, *J. Chem. Soc. Dalton Trans.*, 1995, 3375-3393.
38 A. S. Abd-El-Aziz, S. A. Carruthers, E. K. Todd, T. H. Afifi and J. M. A. Gavina, *J. Polym. Sci., Part A: Polym. Chem.*, 2005, **43**, 1382.
39 A. S. Abd-El-Aziz, E. K. Todd and R. M. Okasha, *Macromol. Containing Met. Met.-Like Elem.*, 2004, **2**, 233.
40 A. S. Abd-El-Aziz, T. H. Afifi, W. R. Budakowski, K. J. Friesen and E. K. Todd, *Macromolecules*, 2002, **35**, 8929.
41 A. S. Abd-El-Aziz, E. K. Todd, G. Ma and J. DiMartino, *J. Inorg. Organomet. Polym*., 2000, **10**, 265.
42 C. Ornelas, J. Ruiz and D. Astruc, *J. Organometal. Chem*., 2009, **694**, 1219.
43 M. Fuentealba, L. Toupet, C. Manzur, D. Carrillo, I. Ledoux-Rak and J.-R. Hamon, *J. Organomet. Chem*., 2007, **692**, 1099.
44 A. Trujillo, M. Fuentealba, C. Manzur, D. Carrillo and J.-R. Hamon, *J. Organomet. Chem.*, 2003, **681**, 150.
45 A.S. Abd-El-Aziz, *Coord. Chem. Rev*., 2002, **233-234**, 177.
46 D. Astruc, *Top. Curr. Chem*., 1992, **160**, 47.
47 D. Astruc, J.-R. Hamon, D. Mandon and F. Moulines, *Pure Appl. Chem*., 1990, **62**, 1165.
48 E. C. Constable and M. D. Ward, *J. Chem. Soc. Dalton Trans.*, 1990, 1405.

49 A. S. Abd-El-Aziz, E. K. Todd, R. M. Okasha, P. O. Shipman and T. E. Wood, *Macromolecules*, 2005, **38**, 9411.

50 U. S. Schubert, C. Eschbaumer, O. Hein and P. R. Andres, *Tetrahedron Lett.*, 2001, **42**, 4705.

51 S. Burazerovic, J. Gradinaru, J. Pierron and T. R. Ward, *Angew. Chem. Int. Ed.*, 2007, **46**, 5510.

52 H. S. Chow, E. C. Constable, C. E. Housecroft, M. Neuburger and S. Schaffner, *Dalton Trans.*, 2006, 2881.

53 L. Zapata, K. Bathany, J.-M. Schmitter and S. Moreau, *Eur. J. Org. Chem.*, 2003, 1022.

54 B. Hess, C. Kutzner, D. van der Spoel and E. Lindahl, *J. Chem. Theory Comput.*, 2008, **4**, 435.

55 D. van der Spoel, E. Lindahl, B. Hess, G. Groenhof, A. E. Mark and H. J. C. Berendsen, *J. Comp. Chem.*, 2005, **26**, 1701.

56 E. Lindahl, B. Hess and D. van der Spoel, *J. Mol. Model.*, 2001, **7**, 306.

57 H. J. C. Berendsen, D. van der Spoel and R. van Drunen, *Comp. Phys. Comm.*, 1995, **91**, 43.

58 C. Oostenbrink, A. Villa, A. E. Mark and W.F. Van Gunsteren, *J. Comp. Chem.*, 2004, **25**, 1656.

59 A. K. Malde, L. Zuo, M. Breeze, M. Stroet, D. Poger, P. C. Nair, C. Oostenbrink and A. E. Mark. *J. Chem. Theory Comput.*, 2011, **7**, 4026.

60 U. Essmann, L. Perera, M. L. Berkowitz, T. Darden, H. Lee and L. G. Pedersen, *J. Chem. Phys.*, 1995, **103**, 8577.

61 J. E. Lennard-Jones, *Proc. R. Soc. London*, 1924, **84**, 457.

62 B. Hess, H. Bekker, H. J. C. Berendsen and J. G. E. M. Fraaije, *J. Comp. Chem.*, 1997, **18**, 1463.

63 G. Bussi, D. Donadio and M. Parrinello, *J. Chem. Phys.*, 2007, **126**, 014101.

64 M. Parrinello and A. Rahman*, J. Appl. Phys.*, 1981, **52**, 7182.

65 S. Nosé and M.L. Klein, *Mol. Phys.*, 1983, **50**, 1055.

66 H. J. C. Berendsen, J. R. Grigera and T. P. Straatsma, *J. Phys. Chem.*, 1987, **91**, 6269.

67 S. Miyamoto and P. A. Kollman, *J. Comp. Chem.*, 1992, **13**, 952.

68 A. D. Becke, *J. Chem. Phys.***,** 1993, **98**, 1372.

69 C. T. Lee, W. T. Yang and R. G. Parr, *Phys. Rev. B*, 1988, **37**, 785.

70 NCIPlot, http://www.chem.duke.edu/~yang/Software/softwareNCI.html (accessed January 26, 2012).

71 E. R. Johnson, S. Keinan, P. Mori-Sanchez, J. Contreras-Garcia, A. J. Cohen and W. Yang, *J. Am. Chem. Soc.*, 2010, **132**, 6498.

72 J. Contreras-Garcia, E. R. Johnson, S. Keinan, R. Chaudret, J.-P. Piquemal, D. N. Beratan and W. Yang, *J. Chem. Theory Comput.*, 2011, **7**, 625.

73 W. Humphrey, A. Dalke and K. Schulten, *J. Mol. Graphics*, 1996, **14**, 33.

74 R. F. W. Bader, *Atoms in Molecules: A Quantum Theory*, Oxford University Press, Oxford, 1990.

75 C. F. Matta, R. J. Boyd, eds., *The Quantum Theory of Atoms in Molecules*, Wiley-VCH, Weinhiem, 2007.

76 AIMAll (Version 11.06.19), Todd A. Keith, TK Gristmill Software, Overland Park, 2011, aim.tkgristmill.com.

77 Gaussian 09, Revision C.01, M. J. Frisch, G. W. Trucks, H. B. Schlegel, G. E. Scuseria, M. A. Robb, J. R. Cheeseman, G. Scalmani, V. Barone, B. Mennucci, G. A. Petersson, H. Nakatsuji, M. Caricato, X. Li, H. P. Hratchian, A. F. Izmaylov, J. Bloino, G. Zheng, J. L. Sonnenberg, M. Hada, M. Ehara, K. Toyota, R. Fukuda, J. Hasegawa, M. Ishida, T. Nakajima, Y. Honda, O. Kitao, H. Nakai, T. Vreven, J. A. Montgomery, Jr., J. E. Peralta, F. Ogliaro, M. Bearpark, J. J. Heyd, E. Brothers, K. N. Kudin, V. N. Staroverov, R. Kobayashi, J. Normand, K. Raghavachari, A. Rendell, J. C. Burant, S. S. Iyengar, J. Tomasi, M. Cossi, N. Rega, J. M. Millam, M. Klene, J. E. Knox, J. B. Cross, V. Bakken, C. Adamo, J. Jaramillo, R. Gomperts, R. E. Stratmann, O. Yazyev, A. J. Austin, R. Cammi, C. Pomelli, J. W. Ochterski, R. L. Martin, K. Morokuma, V. G. Zakrzewski, G. A. Voth, P. Salvador, J. J. Dannenberg, S. Dapprich, A. D. Daniels, Ö. Farkas, J. B. Foresman, J. V. Ortiz, J. Cioslowski, and D. J. Fox, Gaussian, Inc., Wallingford, 2010.

78 A. S. Abd-El-Aziz, T. C. Corkery, E. K. Todd, T. H. Afifi and G. Z. Ma, *J. Inorg. Organomet. Polym. Mater.*, 2003, **13**, 113.

79 J. E. Beves, E. L. Dunphy, E. C. Constable, C. E. Housecroft, C. J. Kepert, M. Neuburger, D. J. Price and S. Schaffner, *Dalton Trans.*, 2008, 386.

80 G. D. Storrier, S. B. Colbran and D. C. Craig, *J. Chem. Soc., Dalton Trans.*, 1997, 3011.

81 E. C. Constable and A. M. W. Cargill Thompson, *New J. Chem.*, 1992, **16**, 855.

82 N. M. Logacheva, V. E. Baulin, A. Y. Tsivadze, E. N. Pyatova, I. S. Ivanova, Y. A. Velikodny and V. V. Chernyshev, *Dalton Trans.*, 2009, 2482.

83 E. C. Constable, K. Harris, C. E. Housecroft, M. Neuburger and S. Schaffner, *Chem. Commun.*, 2008, 5360.

84 A. S. Abd-El-Aziz, L. J. May and A. L. Edel, *Macromol. Rapid Commun.*, 2000, **21**, 598.

85 A. S. Abd-El-Aziz, E. K. Todd, R. M. Okasha and T. E. Wood, *Macromol. Rapid Commun.*, 2002, **23**, 743.

86 A. S. Abd-El-Aziz, R. M. Okasha and T. H. Afifi, *Macromol. Rapid Commun.*, 2004, **25**, 1497.

87 A. S. Abd-El-Aziz, R. M. Okasha and T. H. Afifi, *J. Inorg. Organomet. Polym. Mater.*, 2004, **14**, 269.

88 A. S. Abd-El-Aziz, R. M. Okasha, L. J. May and J. Hurd, *J. Polym. Sci. Part A: Polym. Chem.*, 2006, **44**, 3053.

89 A. S. Abd-El-Aziz, N. M. Pereira, W. Boraie, E. K. Todd, T. H. Afifi, W. Budakowski and K. Friesen, *J. Inorg. Organomet. Polym. Mater.*, 2005, **15**, 497.

90 A. S. Abd-El-Aziz, P. O. Shipman, P. R. Shipley, B. N. Boden, S. Aly and P. D. Harvey, *Macromol. Chem. Phys.*, 2009, **210**, 2099.

91 N. Mahalakshmi and R. Rajavel, *Asian J. Biochem. Pharm. Res.*, 2011, **1**, 525.

92 D. W. Thomas and A. E. Martell, *J. Am. Chem. Soc.*, 1959, **81**, 5111.

93 A. S. Abd-El-Aziz and S. Bernardin, *Coord. Chem. Rev.*, 2003, **203**, 219.

94 J. M. Fritsch, G. C. Curthoys and E. A. Magnussonlb, *J. Am. Chem. Soc.*, 1970, **92**, 2991.

95 D. A. Estrin, O. Y. Hamra, L. Paglieri, L. D. Slep and J. A. Olabe, *Inorg. Chem.*, 1996, **35**, 6832.

96 M. Diefenbach, C. Trage and H. Schwarz, *Helv. Chim. Acta*, 2003, **86**, 1008.

97 A. S. Abd-El-Aziz and I. Manners, *J. Inorg. Organomet. Polym. Mater.*, 2005, **15**, 157.

98 J. W. Nicholson, *The Chemistry of Polymers*, Royal Society of Chemistry, Cambridge, 1991.

99 D. A. Skoog, F. J. Holler and S. R. Crouch, *Principles of Instrumental Analysis*, Thomson Brooks/Cole: Belmont, 2007.